Equation of state of solid molecular H_2 and D_2 at 5 K

Joop van Straaten and Isaac F. Silvera
Lyman Laboratory of Physics, Harvard University, Cambridge, Massachusetts 02138
(Received 8 July 1987)

The equations of state as well as the index of refraction of solid molecular hydrogen and deuterium are measured to 37 GPa in a diamond-anvil cell. The experimental technique is given in detail. The data are fitted with an equation of state based on an effective intermolecular potential. The resulting equation of state is compared to other experimental data, showing good agreement. The critical pressure for the metal-insulator transition is predicted to be 2.8 Mbar, based on the Herzfeld criterion and our equation of state.

INTRODUCTION

The high-pressure equations of state (EOS), i.e., the relation between pressure, volume, and temperature of solid molecular hydrogen and deuterium, are of great experimental and theoretical interest for several reasons. Hydrogen and deuterium are expected to exhibit metal-insulator transitions at high pressures of order 200–500 GPa.[1] To calculate the critical pressure, knowledge of the high-pressure EOS of solid molecular hydrogens is essential.[2] The larger planets, Jupiter, Saturn, and Uranus are made up mainly of hydrogen under high pressure.[3] The EOS of hydrogen is therefore of special interest for planetary sciences.

A number of techniques have been developed to reach high pressures ($P > 10$ GPa) and measure the EOS of hydrogen and deuterium. High pressure has been generated dynamically, in shock wave experiments[4] or by the method of the metallic Z pinch,[5] and statically in a diamond-anvil cell (DAC). In recent years the EOS has been measured by shock wave velocity measurements,[4] by x-ray photography during compression in a metallic Z-pinch experiment,[5] by Brillouin scattering,[6] and direct volume measurements.[2,7,8] We have used a simple and direct technique to measure the volume of a sample of solid molecular hydrogen or deuterium in a DAC at liquid-helium temperature by a combination of photographic and interferometric methods. These measurements have been published in part in a prior article.[2] In this article we give an analysis which includes new data, as well as an extensive discussion of the precision of our technique. A similar technique has been used by Makarenko *et al.*[9] to estimate the EOS of xenon.

Equations of state of solids are often expressed in Birch-Murnaghan (BM) relations which have been shown to be a useful form for solid hydrogen and deuterium for pressures lower than 2.5 GPa. This form for an EOS is based on a power series expansion of the free energy F in the internal strain ϵ, which is considered to be hydrostatic.[10] We do not expect this form to have the proper behavior to extrapolate to high pressures, where the exponentially repulsive part of the intermolecular potential will be dominant. We shall fit our data and low-pressure data[7] with a curve whose form is based on an effective intermolecular potential.[2] The analytical form of this EOS is derived and the physical relevance of the parameters is discussed. In order to compare our EOS to other experimental data, some of which are for room temperature, we use the Mie-Gruneisen model to calculate the temperature-dependent part of the pressure, using the Debye temperatures Θ_D given in Ref. 7. The EOS of solid hydrogen and deuterium at 0, 77, and 300 K are given in Tables III and IV.

The first part of this article describes the experimental technique. In the second part we shall estimate the errors in the data. Since this has not yet been done in the literature, we shall give a rather detailed analysis. In the third part we shall discuss the analytical form of the EOS. This is followed by a discussion of the results and a comparison to other data. The last part of this article discusses the polarizability as a function of pressure and an estimate for the metal-insulator transition pressure is given.

EXPERIMENTAL TECHNIQUE

Our DAC was placed inside a liquid-helium cryostat with an optical tail. This assembly was designed to permit filling of cryogenic fluids. The DAC, the cryostat, and the method used to load cryogenic fluids are described elsewhere.[11] The gaskets used in these experiments were made of T301 stainless steel. Samples were confined in a cylindrical channel in these gaskets as shown in Fig. 1 in cross section. One or more ruby grains of dimensions smaller than 5 μm were placed inside the sample hole to make *in situ* pressure measurements, using the calibrated pressure dependence of the ruby R line in fluorescence.[12] The total volume of the ruby grains is less than 0.1% of the sample volume.

The volume V of the sample for a right cylindrical geometry is

$$V = Ad \ ,$$

where A is the area of the sample hole and d the distance between the diamonds. A was measured by the microphotographic method shown in Fig. 2. The sample was illuminated from both sides; the sample hole and gasket were magnified and imaged outside of the cryo-

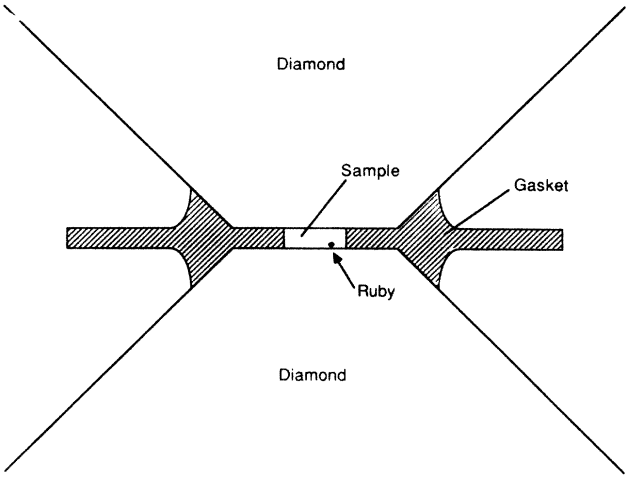

FIG. 1. Cross-sectional view of sample and gasket.

stat by a set of lenses consisting of an 8 cm focal-length (FL) lens in front of the cryostat and a 45 cm FL lens. This image was further magnified by a microscope objective which projected it on the focal plane of a Polaroid film holder. From the photograph the projected area of the sample hole was measured using a planimeter. The area of the diamond culet, defined by the diamond-bevel lines, was also measured and used as a gauge, minimizing possible errors due to changes in magnification.

The distance d between the diamonds was measured by optical interference. The sample was illuminated with a parallel beam of white light; the transmitted light was collected and focused on the entrance slit of a spectrometer as shown in Fig. 3. The diamond surfaces were aligned parallel as explained in Ref. 11 and thus formed a Fabry-Perot etalon. The reflectivity R of the hydrogen-diamond surfaces is[13]

$$R=(n_{\text{diamond}}-n_{\text{H}_2})^2(n_{\text{diamond}}+n_{\text{H}_2})^2 ,$$

where n_{diamond} is the index of refraction of diamond and n_{H_2} is the index of refraction of hydrogen. Because of the high index of refraction of diamond (2.41 for visible light) the reflectance R is high (0.16 for $n_{\text{H}_2}=1$, 0.04 for $n_{\text{H}_2}=1.6$). For incident light I_0, the transmitted light intensity, as a function of wavelength λ, thickness d, and index of refraction n_{H_2} (Ref. 13) is (assuming no absorption)

$$I_{\text{trans}}=I_0/[1+F\sin^2(\delta/2)] ,$$

where $F=4R/(1-R)^2$, $\delta=\pi n_{\text{H}_2}d\cos(\theta)/\lambda$, and θ is the angle the light makes with the diamond culets inside the diamond cell. I_{trans} has maxima at the wave numbers (in cm^{-1})

$$\sigma=1/\lambda=m/(2n_{\text{H}_2}d\cos\theta) ,$$

where m is the order of the maximum. The distance between the maxima in the interference pattern is (assuming no dispersion of n_{H_2})

$$\Delta\sigma=(2n_{\text{H}_2}d\cos\theta)^{-1}=(2n_{\text{H}_2}d)^{-1} \quad \text{for } \theta=0 .$$

The optical path length ($n_{\text{H}_2}d$) can thus be calculated from the interference pattern. An experimental interference pattern of the transmitted light is shown in Fig. 4(a). These interference patterns are divided by the average intensity with the aid of a computer, resulting in interference patterns shown in Fig. 4(b).

The index of refraction n_{H_2} was measured in the following way. The angles θ shown in Fig. 3 and θ_0 (the

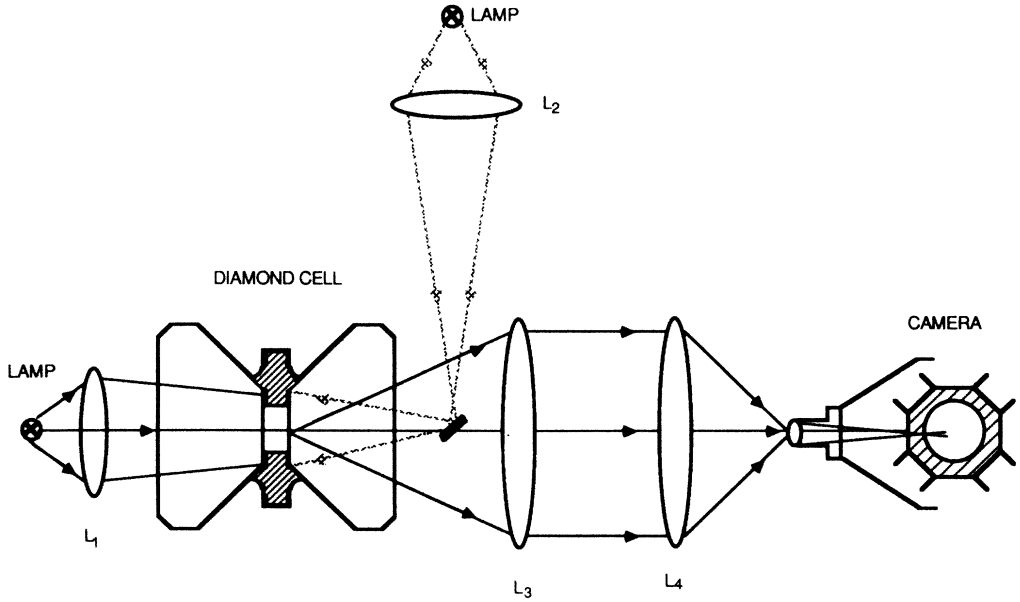

FIG. 2. A schematic drawing of the microphotographic method used to measure the area of the sample.

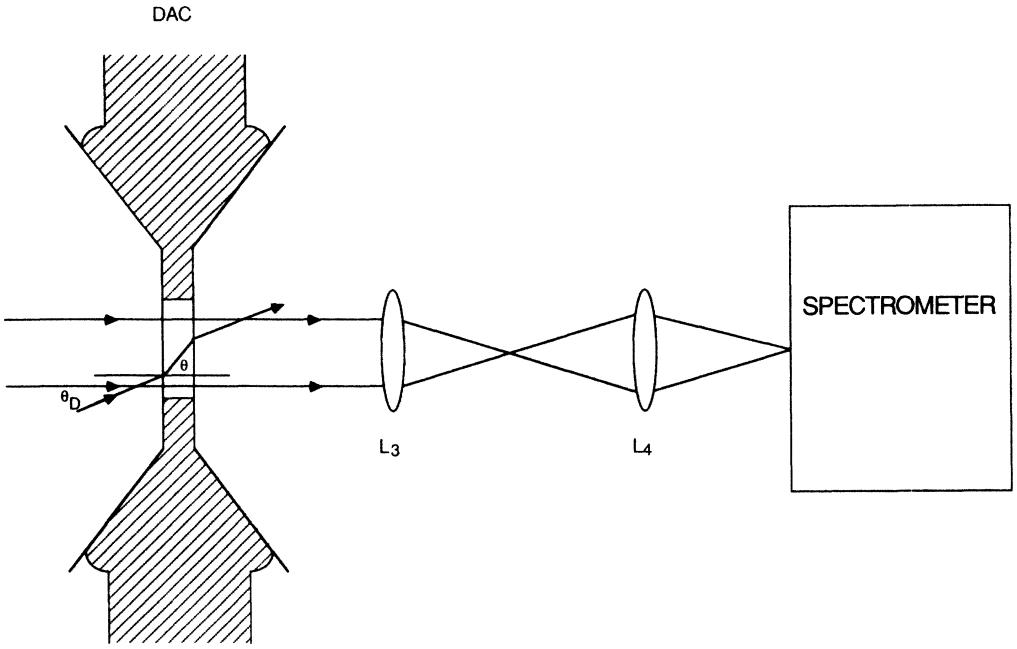

FIG. 3. Schematic drawing of the light paths of incident, transmitted, and reflected light beams.

angle the incident beam makes with the front surface of the diamond, the table) are related via

$$n_{H_2}\sin\theta = n_{\text{diamond}}\sin\theta_D = \sin\theta_0 .$$

The wave number of a fringe maximum as a function of the optical distance $n_{H_2}d$ and the incident angle θ_0 is

$$\sigma = m/(2n_{H_2}d\cos\theta) ,$$

which, for small θ, gives

$$\sigma = \sigma_0(1+0.5\theta_0^2/n_{H_2}^2) ,$$

where $\sigma_0 = m/(2n_{H_2}d)$.

The wave numbers of extrema in the transmission are therefore dependent on θ_0, with a minimum at $\theta_0 = 0$. The second derivative of σ with respect to θ_0 determines n_{H_2} independent of the optical path length. θ_0 was varied by rotating the cryostat and measured by the reflection of a He-Ne laser beam off of a mirror mounted on the cryostat. We typically measured the interference pattern for five to seven different angles and made a computer fit to the above equation. We were thus able to determine the index of refraction n_{H_2} as a function of pressure and to determine d.

SOURCES OF ERROR IN THE VOLUME DETERMINATION

The volume of the sample is taken to be the product of the area A and the distance d. The error in the volume can be split into two contributions, errors in the area and in the thickness. The statistical and systematic errors in these measurements are estimated below.

Area

Errors in the area arise from the limited resolution of the microphotographic method, mainly contributing a statistical error, and from deviations from the right cy-

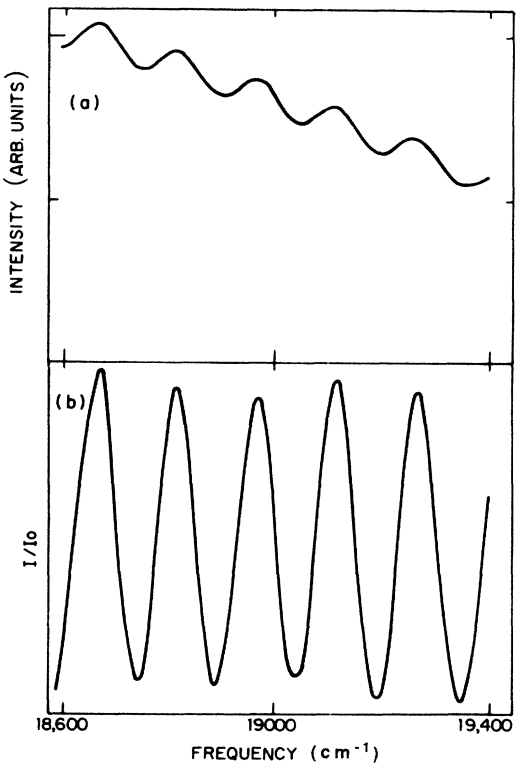

FIG. 4. (a) Experimental interference pattern, (b) normalized pattern.

lindrical geometry, introducing both statistical and systematic errors. The resolution of the microphotographic method, determined mainly by the numerical aperture of the first lens, is approximately 2 μm. To obtain an empirical value for the statistical error caused by the limited resolution and the planimetric area measurement, several photos were taken for most pressures. The spread in area values so measured was on average 2.5% with a maximum of 5%. The average of several photos was taken for the area reducing this statistical error.

Figure 5 illustrates deviations from the right cylindrical geometry. The area A is taken as the projection of the gasket hole on the focal plane of the camera. The sample volume will be underestimated since parts of the sample are hidden from the observer. Figure 5(a) shows a sample hole with tilted walls, the angle of tilt being α. For this geometry the relative error in the volume, $\Delta V/V$, is

$$\begin{aligned}\Delta V/V &= (Ad - V)/(Ad) \\ &= -(\tan\alpha)d/D - 0.33(\tan^2\alpha)d^2/D^2 \\ &= -(\tan\alpha)d/D \quad \text{for small } \alpha \text{ and } d/D \ ,\end{aligned}$$

where D is the diameter of the sample hole. Figure 5(b) shows a sample hole with curved walls. Because in all our experiments the area of the sample hole decreased with increasing pressure and because H_2 is more compressible than the gasket material, a convex rather than concave shape for the walls is assumed. The volume of a sample hole with diameter D, thickness d, and walls with radius of curvature R is

$$\begin{aligned}V = \pi/4\{ &(D+R)^2 d - 2R^2(D+R)[d/(2R)\cos\xi + \xi] \\ &+ R^2[d/3(\cos 2\xi + 2)]\} \ ,\end{aligned}$$

where $\xi = \arcsin(d/2R)$. The maximum curvature of the walls is $R = d/2$. The sample volume for this geometry is

$$V = \pi/4[D^2 d + d^2 D(1-\pi/4) + d^3(1/3 - \pi/8)] \ .$$

The error in the volume, $\Delta V/V$, is

$$\Delta V/V = -d/D(1-\pi/4) - d^2/D^2(1/3 - \pi/8) \ .$$

Figure 5(c) shows a sample hole with tilted, curved walls, showing that to some extent the errors may compensate.

The ratio of the thickness d to the diameter D increased in our experiments on H_2 from approximately 0.16 at 3 GPa to 0.25 at 30 GPa. For the D_2 experiment this ratio was 0.16 at 3 GPa, as for H_2, but due to a sudden change in diameter and thickness decreased at 13 GPa to 0.07. Except for this sudden increase in diameter at 13 GPa the diameter decreased as a function of pressure. The estimated maximum errors at 30 GPa for H_2 are

$$\Delta V/V = -0.06 \quad \text{(curved walls)} \ ,$$

$$\Delta V/V = -0.25\tan\alpha \quad \text{(tilted walls)} \ .$$

This last maximum error is dependent on the tilt angle α. To obtain an empirical estimate of this error we used an electron microscope to study a gasket that had undergone one pressure cycle to 30 GPa before failure of one of the diamonds. The thickness to diameter ratio for this gasket was 0.25. The error in the volume was estimated to be a maximum of 4%.

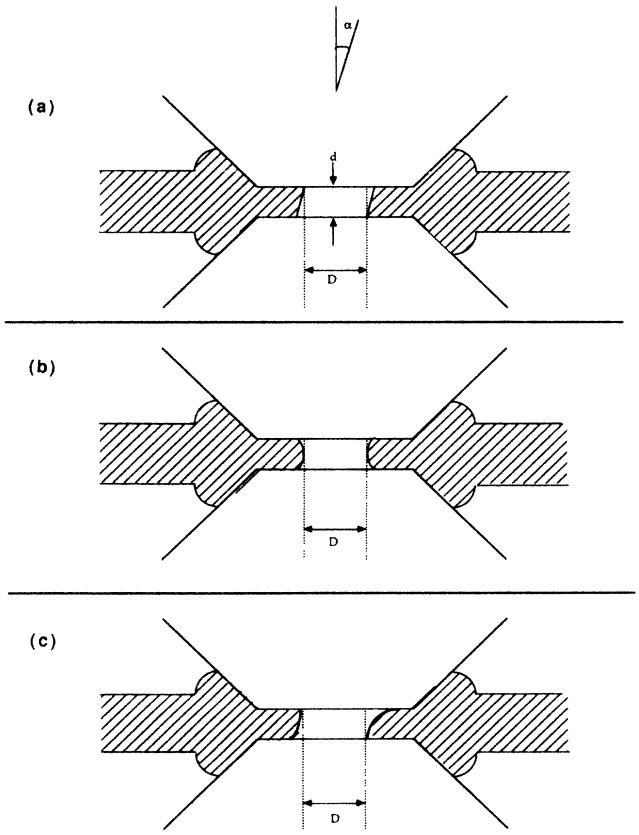

FIG. 5. (a) Cross-sectional and top view of a sample hole which is tilted by an angle α. D denotes the sample hole diameter, d denotes the hole thickness. (b) Cross sectional view of sample with curved, convex walls. (c) Cross sectional view of sample hole with tilted, curves walls.

Thickness d

The thickness d is calculated from the optical path length $n_{H_2}d$ and from the index of refraction n_{H_2} as a function of pressure. Errors may be caused by errors in the optical path length and/or the index of refraction.

Optical path length

The optical path length is calculated from the interference pattern. The error is reduced substantially by measuring several extrema. A typical error is 0.2%. This statistical error is an order of magnitude less than the statistical error in the area.

Systematic errors in the measured optical path length may be introduced by cupping of the diamonds and by dispersion in the index of refraction. Under pressure the diamond faces will cup as shown in Fig. 6. This will effect the interference pattern. The distance d is a function of the distance r to the center of the diamond faces

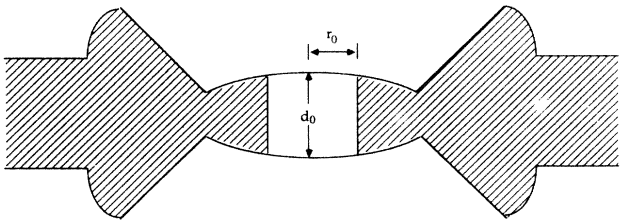

FIG. 6. Cross-sectional view of sample hole showing cupped diamonds.

$$d(r)=d_0+\left[\frac{1}{2}\frac{\partial^2 d}{\partial r^2}\right]r^2+\text{higher orders} ,$$

where d_0 is the distance between the diamonds at the center. The volume of the sample is

$$V=\int_0^{r_0}2\pi d(r)r\,dr=\pi r_0^2\left[d_0+\frac{1}{4}\frac{\partial^2 d}{\partial r^2}r_0^2\right] ,$$

where r_0 is the radius of the sample hole. The transmitted light intensity I_t, as a function of r, is

$$I_t=I_0/[1+F\sin^2(\delta/2)]\approx I_0(1-\tfrac{1}{2}F+\tfrac{1}{2}F\cos\delta) ,$$

where δ is $4\pi n_{H_2}d(r)/\lambda$. The total intensity of the transmitted light is

$$I_{\text{trans}}=\int_0^{r_0}2\pi I_t(r)r\,dr .$$

Substituting I_t in the integration we find after some arithmetic that

$$I_{\text{trans}}=I_0(1-\tfrac{1}{2}F)\pi r_0^2+\tfrac{1}{2}\pi r_0^2 I_0 F(\sin\Delta/\Delta)\cos\delta_0 ,$$

where Δ is

$$4\pi n_{H_2}\left[\frac{1}{4}\frac{\partial^2 d}{\partial r^2}r_0^2\right]\Big/\lambda$$

and δ_0 is

$$4\pi n_{H_2}\left[d_0\left[\frac{1}{4}\frac{\partial^2 d}{\partial r^2}\right]r_0^2\right]\Big/\lambda .$$

The periodicity of the interference spectrum of the transmitted light is therefore

$$\Delta\sigma=\left[2n_{H_2}\left[d_0+\frac{1}{4}\frac{\partial^2 d}{\partial r^2}r_0^2\right]\right]^{-1} ,$$

and the thickness defined by this periodicity is

$$d=d_0+\frac{1}{4}\frac{\partial^2 d}{\partial r^2}r_0^2 .$$

The volume calculated from this thickness d is

$$V=\pi r_0^2 d=\pi r_0^2\left[d_0+\frac{1}{4}\frac{\partial^2 d}{\partial r^2}r_0^2\right] ,$$

equal to the sample volume. Cupping of the diamonds therefore produces a decrease in the contrast of the interference pattern and a long-wavelength modulation on the interference pattern but, neglecting higher-order terms, does not introduce a systematic error in the volume. The diamonds may also be slightly tilted, which will decrease the fringe contrast, but not introduce a systematic error in the volume determination.

A different systematic error in the optical path length may arise due to dispersion in the index of refraction. The distance (in cm^{-1}) between two successive extrema is

$$\Delta\sigma=m_2/(2n_2d)-m_1/(2n_1d) ,$$

where m_2 is the order of the second extremum and is m_1+1, and n_2 is the index of refraction at the wave number of the second extremum and is approximately $n_1+(\partial n/\partial\sigma)\Delta\sigma$. Substituting we find

$$(2nd)^{-1}\simeq\Delta\sigma\left[1+\frac{\partial n}{\partial\sigma}\sigma_1/n\right] ,$$

where σ_1 is the wave number of the first extremum. Due to dispersion in the index of refraction, the optical path length is underestimated. The index of refraction is related to the polarizability α by the Lorentz-Lorenz relation

$$(n^2-1)/(n^2+2)=\tfrac{4}{3}\pi(N_A/V)\alpha ,$$

where N_A is Avogadro's number and V the molar volume. In the simple oscillating shell model[13] α is given by

$$\alpha(\sigma)=Z_i e^2/m(\sigma_0^2-\sigma^2) ,$$

where σ_0 is the frequency of vibration of the atomic shell, Z_i the atomic number, e the charge, and m the mass of the electrons of the shell. We write $\alpha=F_0/(\sigma_0^2-\sigma^2)$, where σ_0 can be seen as an average electronic transition frequency. Substituting this relation for α in the L-L relation and differentiating both sides gives

$$\frac{\partial n}{\partial\sigma}\sigma/n=(n^2+2)(n^2-1)/(3n^2)\sigma^2/(\sigma_0^2-\sigma^2) .$$

The gas value for σ_0 is 114 000 cm^{-1},[14] and σ is approximately 18 000 cm^{-1} (n is given below as a function of pressure). Substituting, we find the dispersion in the index of refraction, assuming that σ_0 is pressure independent, to introduce a systematic underestimate of the optical path length of 1.75% at 3 GPa to 3% at 36 GPa, thus introducing under this assumption a systematic deviation in the relative volumes of $\simeq 1.3\%$.

Index of refraction n_{H_2}

The index of refraction n_{H_2} is measured independent of the optical distance $n_{H_2}d$. Figure 7 shows the measured n_{H_2} and n_{D_2} as a function of pressure. The error bars in the index of refraction measurements are relatively large. Because of this no distinction has been made between measurements on H_2 and D_2. The pre-

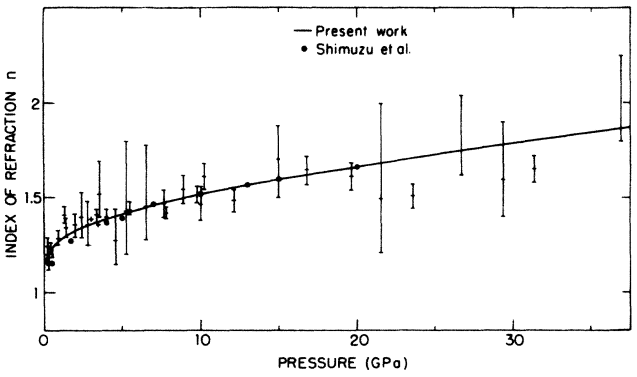

FIG. 7. Index of refraction n of H_2 and D_2 as a function of pressure. The line is the smoothing curve (see text). Upper limits on some of the points were determined from the fringe contrast.

cision was restricted by the limited angle ($-7° < \theta_0 < 7°$) under which the cryostat could be rotated. The errors also become larger for higher pressures because the index of refraction of hydrogen increases, thereby decreasing the fringe contrast, in addition to the decrease due to cupping of the diamonds. In some of our more recent measurements the diamond faces were coated with a partially transparent coating of Cr, thus removing the dependence of the contrast on n_{H_2}. Shimuzu *et al.*[6] measured the index of refraction by Brillouin scattering up to 20 GPa. These measurements are indicated in Fig. 7 by solid circles. To obtain an analytic form of n_{H_2} as a function of pressure we used the following smoothing curve:

$$n_{H_2,D_2} = 0.828(1.694+P)^{0.0316} - 0.708 + 0.001\,022\,9P \ ,$$

where P is in units of 10^8 Pa.[15] The form of this curve was chosen such that the polarizability as given by the L-L relation is a constant or decreasing function of pressure. This smoothing curve fits our data as well as the data of Shimuzu *et al.* This smoothing curve for n can introduce systematic errors. Since the curve is within 0.7% of other measurements of n_{H_2}, both at high[6] and at zero pressure,[16] we estimate the error to be $< 1.0\%$.

To conclude, systematic and statistical errors in the volume can be introduced by several causes. The most important errors are systematic errors in the areal measurements. We did not have enough experimental information to try to correct our EOS to minimize the impact of systematic errors.

We compare to xenon, where Makarenko *et al.*[9] found a fit with the EOS of Ross and McMahan[17] with a 1.5% mean deviation between 10 and 60 GPa. At 60 GPa the thickness-to-diameter ratio was 0.20. X-ray diffraction studies on solid xenon[18] showed the EOS of Ross and McMahan to give slightly (1–2 %) smaller volumes than experimental. However, xenon is less compressible than H_2 and the systematic error for H_2 could be larger for a similar thickness-to-diameter ratio.

ANALYTIC FORM OF THE EOS

We have fit our measurements to an analytic form. The principal objective is to find a form, governed by the physics of the problem, which can be fit to the data with a small number of parameters and extrapolated to higher pressures without fear of becoming nonphysical. We have chosen an analytical form which incorporates zero-point motion contributions to fit our P-V data,[2] based on an effective intermolecular potential. A rigorous derivation is not used.

The EOS is most easily arrived at by consideration of the free energy. The free energy of a solid is formed of two parts, a static part equal to the lattice potential energy, and a dynamic part due to both zero-point motion (ZPM) and lattice excitations. Writing

$$F = F_{\rm stat} + F_{\rm ZPM} + F(V,T) \ ,$$

the pressure P is given by

$$P = \frac{-\partial F}{\partial V} = P_{\rm stat} + P_{\rm ZPM} + P(V,T) \ .$$

The static lattice energy is, neglecting three-body interactions, the sum of the intermolecular interactions over the lattice. Considering nearest-neighbor (NN) interactions only, we can write

$$F_{\rm stat} = ZN_A\Phi(R) \ ,$$

where $2Z$ denotes the number of nearest neighbors, N_A is Avogadro's number, R is the intermolecular nearest-neighbor distance, and $\Phi(R)$ is the intermolecular interaction potential. This approximation for the lattice energy will be better for the short-range repulsive core, where NN interactions are dominant, than for the long-range attractive part.

The zero-point motion energy is[19]

$$F_{\rm ZPM} = \tfrac{3}{2}N_A\hbar\langle\omega\rangle \ ,$$

where $\langle\omega\rangle$ is the first moment of the vibration spectrum. For a Debye spectrum $F_{\rm ZPM}$ is given by[19]

$$F_{\rm ZPM} = \tfrac{3}{2}N_A\hbar\langle\omega\rangle = \tfrac{9}{8}N_A\hbar\omega_D \ .$$

In the free-volume theory, in its simplest interpretation given by Lennard-Jones,[20] ω_D is related to the pair potential $\Phi(R)$ via

$$m\omega_D^2 \propto \frac{1}{2R^2}\frac{\partial}{\partial R}\left[R^2\frac{\partial}{\partial R}\Phi(R)\right] \ .$$

Assuming the lattice energy $F_{\rm stat}$ is proportional to $\Phi(R)$, ω_D is given by

$$m\omega_D^2 \propto \nabla^2 F_{\rm stat} \ .$$

We use this theory, which relates the zero-point motion energy and the lattice energy, to derive the analytic form of the zero-point motion contribution to the EOS. The analytical form for the EOS contains several (four) parameters and will be fit to the experimental data, to determine these parameters.

Different intermolecular potentials have been pro-

posed for H_2 and D_2.[21] We use as a basis for our EOS a simplified version of the potential due to Silvera and Goldman,[22]

$$\Phi(R)=A\exp(-\beta R)-Cf(R)/R^6 ,$$

where

$$f(R)=\exp[-(8.24/R-1)^2]$$

is a function which attenuates the attractive van der Waals term at short distance (R in a.u.).

The static pressure $P_{\rm stat}$ is

$$P_{\rm stat}=-\frac{\partial F_{\rm stat}}{\partial V}$$

$$=C_1Y^{-2}\exp(-C_2Y)-C_3f(Y)Y^{-9} ,$$

where $Y=R/R_r$ and R_r is the nearest-neighbor distance at a reference volume V_r. The zero-point motion pressure is

$$P_{\rm ZPM}=\frac{-\partial F_{\rm ZPM}}{\partial V}=\frac{-C_4\partial}{\partial V}(\nabla^2F_{\rm stat})^{1/2}$$

$$=C_4Y^{-2}[J(Y)]^{-1/2}G(Y) ,$$

where

$$J(Y)=C_1[\exp(-C_2Y)](C_2-2/Y)-5C_3f(Y)Y^{-8}$$

and

$$G(Y)=C_1\exp(-C_2Y)(C_2^2-2C_2/Y-2/Y^2)$$
$$-40C_3f(Y)Y^{-9} ,$$

with

$$f(Y)=\exp[-(3.254Y^{-1}V_r^{-1/3}-1)^2] .$$

For simplification $f(Y)$, which is the same attenuation function as the function $f(R)$ given above, is taken as a constant for the differentiations. The EOS at $T=0$ K contains four parameters, C_1-C_4. In a Birch relation V_0, the zero-pressure volume is an independent variable; in this EOS we use a reference volume V_r which is not an independent variable. V_r is taken as 20 cm^3/mole for both H_2 and D_2. C_1 and C_2 are related to the parameters α and β in the exponentially repulsive part of the intermolecular $\Phi(R)$,

$$C_1=C_2N_AZA/(3V_r) ,$$

$$C_2=\beta R_r ,$$

where A is e^{α}. C_3 is related to parameter C in the attractive part of $\Phi(R)$,

$$C_3=2N_AZC/V_r .$$

Taking $F_{\rm ZPM}=\frac{9}{8}\hbar N_A\omega_D$ and $m\omega_D^2=\nabla^2F_{\rm stat}$, C_4 is calculated to be

$$C_4=\tfrac{3}{4}\hbar/R_r[N_A/(3mZV_r)]^{1/2} .$$

If V_r is taken equal for H_2 and D_2, we expect C_1-C_3 to be (approximately) the same for both isotopes, and $C_4(H_2)/C_4(D_2)=\sqrt{2}$.

The pressure at $T=0$ K is

$$P=P_{\rm stat}+P_{\rm ZPM} .$$

All our data were taken at liquid-helium temperature, so $P(V,T)$, the thermal pressure, is negligible, since $\Theta_D\gg 5$ K. To compare our data to other experimental data, some of which have been taken at room temperature, the thermal pressure is calculated using the Mie-Gruniesen model. The thermal pressure can be given in this model as a function of a characteristic temperature Θ_D and the Gruneisen parameter $\gamma(V)$:

$$P(V,T)=\gamma(V)9N_Ak_b/\Theta_D^3(V)T^4\int_0^{x_d}x^3/(e^x-1)dx ,$$

where

$$\gamma(V)=\frac{-\partial\ln\Theta_D}{\partial\ln V}\ \text{and}\ x_D=\Theta_D/T .$$

For Θ_D we use an empirical function proposed by Berkhout and Silvera,[23]

$$\Theta_D=\Pi\exp(D_kb^k),\quad k\geq 0 ,$$

with $b=\ln(V/V_0)$ and V_0 the zero-pressure volume. The parameters used are given in Table I, taken from Ref. 7.

RESULTS

The sample volume is measured as a function of pressure. However, the amount of material in the sample volume is not known. Although this could be calculated from the original size of the sample hole, leakage at low pressures ($P<0.1$ GPa) or precompression could introduce substantial errors. We therefore scale the sample volumes to the known molar volumes of H_2 and D_2 at low pressure ($P<3.0$ GPa) using the EOS of Ref. 7. Typically an experiment consisted of eight volume measurements at pressures between 1.0 and 30 GPa.

We take our data and determine the coefficients C_1-C_4 by minimizing

$$\sigma=\left[\sum(\Delta V_k/V_k)^2\right]^{1/2} ,$$

where k runs over our data points and over eight points of the EOS given in Ref. 7 between 10 and 20 cm^3/mole. Here ΔV_k is the difference in molar volume between the

TABLE I. The coefficients D_k and V_0 used in the analytic expression for Θ.

	H_2	D_2
D_0	4.5987	4.5525
D_1	−2.2128	−1.836
D_3	−0.611 92	−0.184 48
D_4	−0.0196	
V_0	23.207 (cm^3/mole)	19.95 (cm^3/mole)

TABLE II. The coefficients of the $T=0$ K isotherm, $V_r=20$ cm^3/mole, P in GPa.

	C_2	C_2	C_3	C_4
	10^4 GPa		GPa	10^{-3} GPa$^{1/2}$
H_2	0.6839	9.995	0.3317	5.577
D_2	1.0811	10.531	0.3629	3.902

measured data points and a calculated point of the EOS. The resulting coefficients C_1-C_4 for H_2 and D_2 are given in Table II. The resulting equations of state for $T=0$, 77, and 300 K are given in Tables III and IV for H_2 and D_2, respectively. The EOS for $T=0$ K of D_2 given here is the same as the EOS given in Ref. 2, while for H_2 it differs due to the inclusion of new data points. The EOS given here is somewhat softer at high pressures. This may of course be due to systematic errors as explained above. The difference between the two equations of state is always within the estimated maximum error. In general, C_1-C_3 are roughly equal for H_2 and D_2 as expected, since these coefficients are related to the static lattice energy. C_1 and C_2, the coefficients corresponding to the repulsive part of the potential, are smaller for H_2 than for D_2, because H_2 is slightly softer for high pressures than D_2. The coefficients C_4 are close to the calculated coefficients, which for 12 nearest neighbors are 6.93×10^{-3} (GPa)$^{1/2}$ and 4.9×10^{-3} (GPa)$^{1/2}$ for H_2 and D_2, respectively. The EOS at $T=0$ K is shown in Fig. 8 on a quasilogarithmic scale in which we add 0.1 GPa to the sample pressure. Figure 9 is a deviation plot showing the relative difference between the measured volumes and the EOS, $\Delta V/V$, as a function of volume for H_2 and D_2, respectively. Also shown, by open circles, are selected points of the EOS of solid H_2 and D_2 from Ref. 7. For D_2 no systematic deviation between the EOS and the measured volumes is seen. For H_2 a small positive deviation for volumes greater than 7 cm^3/mole and a small negative deviation for smaller volumes is seen.

TABLE III. EOS for solid H_2 at 0, 77, and 300 K using the analytic from with parameters given in Table II.

	Pressure (GPa)		
V (cm^3/mole)	$T=0$	$T=77$ K	$T=300$ K
20	0.0647		
19	0.0923		
18	0.1313		
17	0.1842		
16	0.2572		
15	0.3587		
14	0.5032	0.5559	
13	0.7071	0.7518	
12	1.005	1.042	
11	1.446	1.473	
10	2.116	2.139	
9	3.165	3.182	
8	4.867	4.879	5.311
7	7.76	7.77	8.15
6	12.97	12.98	13.29
5	23.12	23.12	23.37
4	45.09	45.09	45.24
3	100.7	100.7	100.7
2	281.6	281.6	281.6

TABLE IV. EOS for D_2 at 0, 77, and 300 K using the analytic form with parameters given in Table III.

	Pressure (GPa)		
V (cm^3/mole)	$T=0$ K	$T=77$ K	$T=300$ K
20	−0.0008		
19	0.0118		
18	0.0407		
17	0.0829		
16	0.1444		
15	0.2340		
14	0.3655		
13	0.5602	0.6484	
12	0.8526	0.9328	
11	1.300	1.370	
10	1.998	2.058	
9	3.121	3.169	
8	4.992	5.028	5.873
7	8.250	8.275	9.117
6	14.26	14.28	15.09
5	26.25	26.25	26.98
4	52.80	52.81	53.39
3	121.6	121.6	122.0
2	351.4	351.4	351.4

POSSIBLE MODIFICATION OF THE EOS AT HIGH PRESSURE

We have derived equations of state for H_2 and D_2 based on certain assumptions, namely a simplified Silvera-Goldman potential; the seven coefficients of the potential, α, β, and γ for the repulsive core, and C_6, C_8, C_9, and C_{10} for the long-range interaction are replaced by three, A, and B for the repulsive core, and C for the attractive R^{-6} interaction. The zero-point motion pressure is calculated by a simple model. Next-nearest-neighbor as well as three-body interactions are not con-

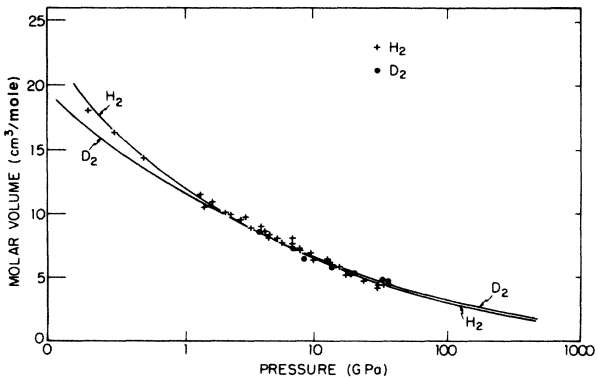

FIG. 8. The $T=0$ K isotherms of H_2 and D_2. Pressures beyond 37 GPa are extrapolations.

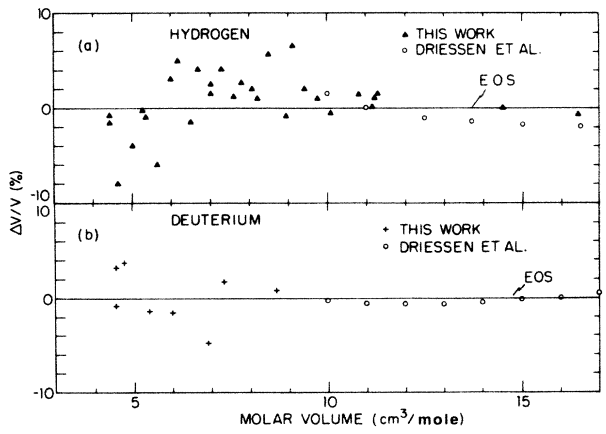

FIG. 9. The relative difference in volume $\Delta V/V$ as a function of the molar volume between the measurements and an analytic EOS given by the horizontal line. Selected points of the EOS of Ref. 7 are given by open circles. (a) H_2; (b) D_2.

sidered. The latter is believed to be responsible for a softer effective pair potential at high pressure.

In this approach we have completely ignored the internal structure of the molecules, which must begin to expose itself as one approaches the molecular-atomic solid transition. A contribution to the EOS which has not been explicitly taken into account arises from the zero-point motion associated with the molecular vibrations, the vibrons. This intramolecular zero-point motion pressure is small, of order 0.001–0.3 GPa in the pressure regime of 0–10 GPa, but not negligible. It is small in the 30–50 GPa region since the vibron frequency goes through a maximum at approximately 30 GPa (Ref. 24) for the Raman-active and 50 GPa (Ref. 25) for the infrared (ir) active vibrons, and as we shall see this pressure is proportional to $\partial V/\partial P$. All of these effects and simplifications are incorporated in C_1–C_4 to some extent.

Raman-scattering experiments at high pressure[24,25] have shown that the pressure dependence of the intramolecular Raman-active vibrational-mode frequencies of H_2 and D_2 do not scale according to the mass ratios. Using the Dunham[26] theory, Wijngaarden *et al.*[24] transformed these vibrational-mode frequencies to a mass independent value. Above approximately 10 GPa the values for H_2 and D_2 diverged. This as yet unexplained phenomena indicates that the influence of the intermolecular interactions on the intramolecular bond is different for the two hydrogens for high pressure. One consequence of this could be that at a given pressure the intramolecular H-H distance differs from the D-D distance. The effective pair potentials can then be different for the two hydrogens, resulting in different equations of state.

For extrapolation of the EOS to higher pressure it should be realized that the intramolecular zero-point motion pressure will give a negative contribution to the total pressure. At pressures above 2 Mbar the vibrational frequencies continue to decrease.[27] We estimate the pressure due to the change of the vibrational-mode frequencies by

$$P(\text{vibron}) = -0.5 N_A \hbar \frac{\partial \nu_{\text{vibron}}}{\partial V}$$

$$= 0.5 N_A \hbar (B/V) \frac{\partial \nu_{\text{vibron}}}{\partial P} ,$$

where B is the bulk modulus and V the molar volume. If we take the Raman-active vibron frequency as a measure for the total intramolecular vibrational energy, we can estimate P_{ZBM}(vibrons) using the measurements of Mao *et al.*[27] up to 150 GPa. P_{ZPM} is approximately 0, −4, and −9 GPa at 50, 100, and 150 GPa total pressure, respectively, for H_2 and 0, −1, and −2 GPa for D_2. This shows that for H_2 between 100 and 150 GPa, the intramolecular modes give an important, negative contribution to the total pressure. which increase with pressure. Because this effect has not been taken into consideration in the EOS we might speculate that at pressures of more than 100 GPa, the EOS for H_2 given here overestimates the pressure.

COMPARISON TO OTHER EXPERIMENTAL DATA

Figure 10 compares the deviation $\Delta V/V$ of other experimental data on the EOS of H_2 with our results, as a function of the molar volume. Several experiments have been done for pressures below 2.5 GPa. Most of these have been reviewed by Driessen *et al.*,[7] and were fitted for $T=0$ K by a BM equation which is compared in Fig. 10 to our $T=0$ K isotherm by curve 1. Recently Ishmaev *et al.*[28] investigated solid para-H_2 by neutron diffraction between 4.2 and 100 K to pressures of 2.4 GPa. Their results are given by curve 5. Above 2.5 GPa the EOS of H_2 has been measured by Matveev *et al.*[5] in a metallic Z pinch to 15 GPa, by Ross *et al.* in shock wave experiments to 76 GPa (Ref. 4) and by Shimuzu *et al.* to 20 GPa by Brillouin scattering.[6] The measurements of Matveev *et al.* are given in Fig. 10 by solid dots. The temperature for this experiment was given as <100 K and their results are compared to our $T=0$ isotherm. The 0 K equation of state for solid H_2

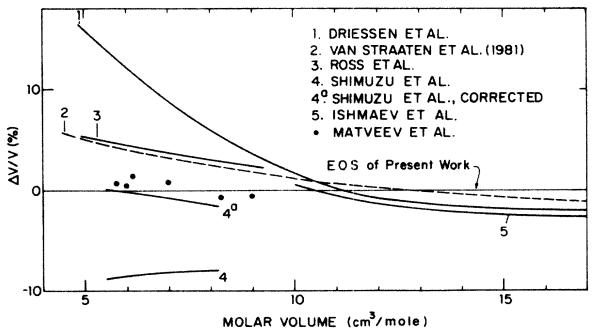

FIG. 10. A comparison of the relative difference in volume $\Delta V/V$ at equal pressure as a function of the molar volume between this work and other data. Our EOS is given by the horizontal axis.

derived by Ross *et al.*[4] is compared to our $T=0$ K isotherm by curve 3. The $T=300$ K isotherm derived from the Brillouin measurements by Shimuzu *et al.* is compared to the $T=300$ K isotherm of our EOS by curve 4. Perhaps the most accurately determined high-pressure point is from the recent x-ray study of Hazen *et al.*[29] who found $V=7.994\pm0.015$ cm^3/mole at 5.40 GPa and $T=300$ K. Correcting our measurement to 300 K Table III gives $P=5.33$ GPa at this density. More appropriately, at a pressure of 5.40 GPa we find a deviation of $\Delta V=0.019$ cm^3 or $\Delta V/V=2.38\times10^{-3}$ in excellent agreement. Finally, for comparison, the EOS for H_2 given by us in Ref. 2 is given by the dashed curve 2.

These measurements, taken independently and using different techniques, overlap within 5% in volume, except for the measurements by Shimuzu *et al.*[6] Our EOS gives slightly higher (approximately 2%) larger volumes than other experimental data for molar volumes larger than 11 cm^3/mole. For this regime we recommend the EOS of Driessen *et al.* This EOS, when extrapolated, gives a substantially larger volume than the other measurements, but as explained above, a BM equation is not the best analytic form of the EOS for extrapolation. For decreasing molar volume an increasing difference is seen between our EOS and the EOS given by Ross *et al.*, up to approximately 5%. This difference is not outside the estimated maximum error. The EOS of Ross *et al.* is dependent on data from shock experiments taken on H_2 and D_2. These experiments comprise single-shock experiments on H_2 to a pressure of 20 GPa, corresponding to a molar volume of 7.1 cm^3/mole, and double-shock experiments on D_2, corresponding to a molar volume of 3.8 cm^3/mole. From these data one effective potential for both H_2 and D_2 was calculated. For small molar volume the resulting effective potential is therefore mainly determined by the D_2 experiments. Differences between the effective potentials of H_2 and D_2 for intermolecular distances smaller than those probed in the H_2 experiments could explain the difference between our EOS and the EOS given by Ross *et al.* Comparing the measured single-shock H_2 molar volumes to the calculated molar volume at high pressures, a small systematic difference can be seen, with the measured volumes being smaller than the calculated volumes.

Shimuzu *et al.* derive an EOS for H_2 from their Brillouin scattering measurements that is substantially different from the other experimental data, as can be seen in Fig. 10. A possible explanation for the difference in the equations of state for solid H_2 is given by Shimuzu in a later article.[30] The hypersonic longitudinal and transverse speed of sound of solid H_2 and the hypersonic speed of sound of liquid H_2 were measured. From these the bulk modulus B is calculated as a function of pressure and by integration of B over pressure the EOS is calculated. The EOS for the solid phase therefore depends on measurements taken in the fluid phase. Chemical contamination of the H_2 in the liquid phase might influence the sound velocities in liquid H_2 and the resulting EOS for both the fluid and solid phase. It was indeed noticed that the sound velocity in H_2 decreased as a function of time, probably due to progressive contamination. Shimuzu estimates this effect to contribute a constant shift in volume of 0.4 cm^3/mole for solid H_2. The EOS of solid H_2 when corrected for this effect is given by curve 4a, showing improved agreement with our EOS and other data. It should be remarked here that some of these data are for parahydrogen and some for normal hydrogen. However, at high pressure the ortho-para effects on the EOS should be negligible. In conclusion, we believe that reasonable agreement between our EOS and other data, with the exception of the uncorrected EOS of Shimuzu, exists.

POLARIZABILITY AND THE METAL-INSULATOR TRANSITION

The polarizability, α, of solid H_2 and D_2 can be calculated as a function of pressure using the Lorentz-Lorenz relation

$$(n^2-1)/(n^2+2)=\tfrac{4}{3}\pi(N_A/V)\alpha\ ,$$

where N_A is Avogadro's number and V the molar volume. Using the smoothing curve for n given above, the EOS of Driessen *et al.* for molar volumes less than 11 cm^3, and for smaller volumes the EOS given here for H_2 at $T=0$ K, we find the polarizability to be essentially a decreasing function of pressure. In Fig. 11 we show the polarizability of H_2 as a function of density. The static values of α measured by several workers are given in Fig. 11: Peck and Huang,[14] Diller,[31] and Younglove[32] (curve 1 for the fluid phase, curve 2 for the solid) and are approximately 8.03×10^{-25} cm^3. The dynamical values at 5145 Å were measured by Peck and Huang (open triangle) and Diller (open square) and are approximately 8.27×10^{-25} cm^3. Shimuzu *et al.*[6] estimate α to be pressure insensitive in the fluid phase with $\alpha=8.17\times10^{-25}$ cm^3 and to show a discontinuous decrease on the fluid-solid phase transition followed by a continuous decrease in the solid phase to 7.12×10^{-25} cm^3. Using the corrected EOS of Shimuzu[30] α is given by curve 4a. The polarizability from our work is given by curves 5 and 6. [Curve 5 gives α for low pressures ($P<1.5$ GPa) using the EOS of Driessen *et al.*; curve 6 gives α for higher pressures.] In general the polarizability is a decreasing function of pressure. At pressures below 1.5 GPa α determined here agrees within experimental error to the values as measured by Peck and Huang and Diller.

The insulator-metal transition of H_2 has been the focus of considerable research ever since Wigner and Huntington[33] proposed a structural transition from a diatomic to a monatomic metallic phase. Since then many predictions of the insulator-metal transition have been made. Friedly and Ashcroft[34] have predicted a continuous insulator-metal transition in the molecular solid, with band crossing at a volume of 2.4 cm^3/mole, and a pressure of 210 GPa. Monte Carlo simulations by Ceperley and Adler[35] in both the molecular and atomic phase are in reasonable agreement with our EOS and

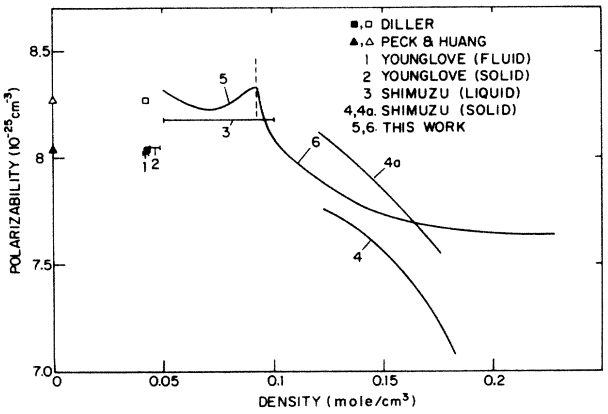

FIG. 11. Polarizability of H_2 as a function of density.

give a transition pressure and volume of 2.8 Mbar and 2.1 cm^3/mole. Recently Min *et al.*[36] predicted a transition from a diatomic insulator to a diatomic metal state at a volume of 2.33 cm^3/mole, corresponding to a pressure of 170 GPa, followed by a structural phase transition to a monoatomic metallic phase at 400 GPa. The highest pressure reached for H_2 and D_2 in a DAC is 147 GPa (Ref. 27), for which the sample remained transparent.

Recently the insulator-metal transitions of several molecular and ionic solids under high pressure, e.g., I_2,[37] HI,[38] BaTe,[39] and CsI,[40] have been investigated. For these solids the Herzfeld criterion accurately predicts the metal-insulator transition. In the Herzfeld approach the dielectric constant and also the index of refraction become infinite at the insulator-metal transition. It then follows from the Lorentz-Lorenz relation that the metallization volume V_m is $\frac{4}{3}\pi N_A \alpha$. Using the Herzfeld criterion we estimate the metallization volume to be 2.02 cm^3/mole, corresponding to a pressure of 280 GPa. There have been some claims of metallization of hydrogen in dynamic compression experiments.[41,42] However, we believe that a satisfactory proof of metallization with reliable measurements of physical properties should be done statically under equilibrium conditions. Techniques to reach pressures of the required magnitude on hard materials, using a DAC, have recently been developed.[43] However, extending these techniques to a soft material such as hydrogen remains a challenging problem.

ACKNOWLEDGMENTS

We would like to thank R. J. Wijngaarden for help in our earlier experiments. This research was supported by National Science Foundation (NSF) Grant DMR-8600995 and by De Stichting voor Fundamental Onderzoek der Materie (FOM) of the Netherlands.

[1]M. Ross and C. Shishkevich, Rand Corporation Report No. R-2056-ARPA, 1977 (unpublished).
[2]J. van Straaten, I. F. Silvera, and R. J. Wijngaarden, Phys. Rev. Lett. **48**, 97 (1982).
[3]W. B. Hubbard and R. S. Moluchowski, Space Sci. Rev. **14**, 599 (1973).
[4]W. J. Nellis, M. Ross, A. C. Mitchell, M. van Thiel, D. A. Young, F. H. Ree, and R. J. Trainor, Phys. Rev. A **27**, 608 (1983).
[5]V. V. Matveev, I. V. Medvedeva, V. V. Prut, P. AS. Suslov, and S. A. Shibaev, Pis'ma Zh. Eksp. Teor. Fiz. **39**, 219 (1984) [Sov. Phys.—JETP Lett. **39**, 261 (1984)].
[6]H. Shimuzu, E. M. Brody, H. K. Mao, and P. M. Bell, Phys. Rev. Lett. **47**, 128 (1981).
[7]A. Driessen and I. F. Silvera, J. Low Temp. Phys. **54**, 361 (1984).
[8]D. H. Liebenberg, R. L. Mills, and J. C. Bronson, Phys. Rev. B **18**, 4526 (1978).
[9]I. Makarenko, G. Weill, J. P. Itie, and J. M. Besson, Phys. Rev. B **26**, 7113 (1982).
[10]F. Birch, Phys. Rev. **71**, 809 (1947).
[11]I. F. Silvera and R. Wijngaarden, Rev. Sci. Instrum. **56**, 121 (1985).
[12]We use the ruby calibration scale of H. K. Mao, P. M. Bell, J. Shaner, and D. Steinberg, J. Appl. Phys. **49**, 3276 (1978), along with the observation of a shift in the scale by P. A. Noah and W. A. Holzapfel, in *Proceedings of the Sixth AIRAPT International High Pressure Conference, Boulder, Colorado, 1977*, edited by K. D. Timmerhaus and M. S. Barber (Plenum, New York, 1979).
[13]M. Born and E. Wolf, *Principles of Optics* (Pergamon, Oxford, 1980), Chap. 7.
[14]E. R. Peck and S. Huang, J. Opt. Soc. Am. **67**, 1551 (1968).
[15]This curve differs slightly from the curve given in Ref. 2, as new data points have been included.
[16]B. A. Wallace and H. Meyer, J. Low Temp. Phys. **15**, 297 (1974).
[17]M. Ross and A. K. McMahan, Phys. Rev. B **21**, 1658 (1980).
[18]K. Asaumi, Institute for Solid State Physics, University of Tokyo Report No. 1413, Series A (1984).
[19]C. Domb and L. Slater, Philos. Mag. **43**, 1083 (1952).
[20]J. E. Lennard-Jones and A. F. Devonshire, Proc. R. Soc. London, Ser. A **163**, 53 (1937).
[21]See, for example, I. F. Silvera, Rev. Mod. Phys. **52**, 393 (1980).
[22]I. F. Silvera and V. V. Goldman, J. Chem. Phys. **69**, 4209 (1978).
[23]P. J. Berkhout and I. F. Silvera, J. Low Temp. Phys. **48**, 4181 (1979).
[24]R. J. Wijngaarden, A. Lagendijk, and I. F. Silvera, Phys. Rev. B **26**, 4957 (1982).
[25]H. K. Mao, J. A. Xu, and P. M. Bell, Carnegie Geophysical Institute Yearbook **83**, 366 (1983).
[26]J. L. Dunham, Phys. Rev. **41**, 721 (1932).
[27]H. K. Mao, P. M. Bell, and R. J. Hemley, Phys. Rev. Lett. **55**, 99 (1985).
[28]S. N. Ishmaev, I. P. Sadikov, A. A. Chernyshov, B. A. Vindryaevskii, V. A. Sukhoparov, A. S. Telepnav, and G. V. Kobelev, Zh. Eksp. Teor. Phys. **84**, 394 (1983) [Sov. Phys.—JETP **57**, 229 (1983)].

[29]R. M. Hazen, H. K. Mao, and L. W. Finger, Bull. Am. Phys. Soc. **32**, 798 (1987).
[30]H. Shimuzu, in *Proceedings of the 9th International AIRAPT Conference, Albany, 1983,* edited by C. Homan, R. K. MacCrone, and E. Whalley (North-Holland, New York, 1984), Part 2, pp. 57–60.
[31]D. E. Miller, J. Chem. Phys. **49**, 3096 (1968).
[32]B. A. Younglove, J. Chem. Phys. **48**, 4181 (1968).
[33]E. Wigner and H. B. Huntington, J. Chem. Phys. **3**, 764 (1935).
[34]C. Friedli and N. W. Ashcroft, Phys. Rev. B **16**, 662 (1977).
[35]D. Ceperley and B. Alder (unpublished).
[36]B. I. Min, H. J. F. Jansen, and A. J. Freeman, Phys. Rev. B **33**, 6383 (1986).
[37]K. Takemaura, Y. Fujui, S. Minomura, and O. Shimomura, Solid State Commun. **30**, 13 (1979); N. Sakai, T. Kajiwara, K. Tsuji, and S. Minomura, Rev. Sci. Instrum. **53**, 499 (1982).
[38]J. van Straaten and I. F. Silvera, Phys. Rev. Lett. **57**, 766 (1986).
[39]T. A. Grzbowski and A. L. Ruoff, Phys. Rev. Lett. **53**, 489 (1984).
[40]R. Reichlin, M. Ross, S. Martin, and K. A. Goettel, Phys. Rev. Lett. **56**, 2858 (1986).
[41]R. S. Hawke, T. J. Burgess, D. E. Duerre, J. G. Hoebel, R. N. Keeler, H. Klapper, and W. C. Wallace, Phys. Rev. Lett. **41**, 994 (1978).
[42]F. V. Grigor'ev, S. B. Kormer, O. L. Mikhailova, A. P. Tolochko, and V. V. Urlin, Pis'ma, Zh. Eksp. Teor. Fiz. **16**, 286 (1972) [Sov. Phys.—JETP Lett. **16**, 201 (1972)].
[43]J. A. Xu, H. K. Mao, and P. M. Bell, Science **232**, 1404 (1986).